Organic Electronics 50 (2017) 347–358

Contents lists available at ScienceDirect

Organic Electronics

journal homepage: www.elsevier.com/locate/orgel

Magnetic field effects in Alq_3-based OLEDs investigated by electrical impedance spectroscopy

Oswaldo Nunes-Neto [a], Augusto Batagin-Neto [b, *], Douglas M.G. Leite [c], Frank A. Nüesch [d], Carlos F.O. Graeff [a, e]

[a] Universidade Estadual Paulista (UNESP), POSMAT - Programa de Pós-Graduação em Ciência e Tecnologia de Materiais, Faculdade de Ciências, Bauru, Brazil
[b] Universidade Estadual Paulista (UNESP), Câmpus Experimental de Itapeva, Brazil
[c] Instituto Tecnológico de Aeronáutica, Divisão de Ciências Fundamentais, Departamento de Física, Campus CTA, São José dos Campos, São Paulo, Brazil
[d] EMPA, Laboratory for Functional Polymers, Swiss Federal Laboratories for Materials Science and Technology, Überlandstrasse 129, CH-8600 Dübendorf, Switzerland
[e] Universidade Estadual Paulista (UNESP), Faculdade de Ciências, Bauru, Brazil

ARTICLE INFO

Article history:
Received 1 May 2017
Received in revised form
17 July 2017
Accepted 3 August 2017
Available online 5 August 2017

Keywords:
Magneto-impedance
Drift-diffusion approach
Organic light emitting diodes

ABSTRACT

The effect of an external magnetic field on electrical impedance was measured on tris-(8-hydroxyquinoline) aluminum (Alq_3) based OLEDs at different temperatures. Magnetic field effects (MFEs) were responsible for significant changes on the real and imaginary components of the impedance, and for the intensification of the negative capacitance (NC) effect. The observed MFEs do not present a strong temperature dependence. Simulations via equivalent circuits and numerical solutions of Boltzmann transport equations in a drift-diffusion approximation and employing small sinusoidal signal analysis indicate that such effects are consistent with an enhancement of the carrier mobilities and a quenching of the recombination rates. Such changes lead to reduced resistance and more intense NC effects on the device. The results were interpreted in terms of the currently accepted OMAR models: electron-hole pair model, triplet-polaron reaction mechanism and bipolaron model.

1. Introduction

Organic magnetoresistance (OMAR) is an intriguing phenomenon where variations in the electrical conductivity of organic materials can be induced by small external magnetic fields. The effect is observed in carbon based materials that typically have a small spin-orbit coupling, with non-magnetic electrodes, and is observed at room temperature for a varied set of polymeric and molecular materials [1].

In addition to the relevance of such magnetic field effect (MFE) for basic science, OMAR has also emerged as a potential tool for different technological applications, including displays [2,3], flexible magnetic field sensors [4,5], spin OLEDs [5], and devices for energy storage [6]. Indeed, in essence OMAR may have an unlimited field of action, for example, in the area of organic-based nanocomposites [7–9]. However, in spite of the academic and technological interest, until now the mechanism associated with this phenomenon is not completely understood.

In general there is a consensus in the literature that the effect is associated with changes promoted by an external magnetic field on the interaction of spin carriers with local fields [10–15]. In the absence of an external magnetic field these local fields have random orientations, so that a significant spin mixing is generally observed between the precursor states that governs the spin carrier dynamics. The application of an external field promotes a reduction in the mixing, leading to changes on the carriers dynamics and consequently on the electrical and optical responses of the devices.

Basically two categories of models have been proposed to explain the origin of OMAR: the bipolaron model [16] and the excitonic models [17–24]. In the excitonic models it is considered that the magnetic field can either modulate the inter-conversion between singlet and triplet electron-hole pairs (electron-hole pair model) or interfere in reactions involving triplet excitons and free carriers (triplet-polaron reaction model); while in the bipolaron model it is proposed that the response of the device depends on the formation of bipolarons during the hopping processes in the

* Corresponding author.
E-mail address: abatagin@itapeva.unesp.br (A. Batagin-Neto).

http://dx.doi.org/10.1016/j.orgel.2017.08.003
1566-1199/

organic material.

As a matter of fact, a variety of physical processes that can be influenced by an external magnetic field are supposed to happen in OLEDs under working conditions [25–27]. Since these processes in general present distinct response times, the use of techniques in the frequency domain can be a very interesting tool to identify the MFEs that indeed dominate the electrical response of the device in distinct frequency ranges. Moreover, additional information can also be obtained by the phase analysis of these responses. In this context, OMAR studies in the frequency domain have been carried out [26–32].

Wagemans et al. [28], Janssen et al. [30] and Wang et al. [29] have investigated frequency dependence of OMAR in Alq_3-based devices by applying a DC bias voltage and a modulated magnetic field. They have observed that the magnetoconductance decreases when the frequency is increased, and this dependence is stronger at lower voltages. The role of minority carriers dynamics was highlighted in these works, as well as that negative capacitance could be associated with the effect. Since magnetic field modulation was used, it was difficult to understand and separate the electrical and magnetic frequency contributions.

These setbacks were overcome by Rogachev and coworkers that investigated the MFEs induced on the admittance spectra of MEH-PPV-based OLEDs under weak static magnetic fields [31,32]. In this approach it was considered that the external magnetic field induces a constant change on physical parameters of the device, allowing a more direct interpretation of the electrical responses. Djidjou et al. identified that the MFE observed on their device could be attributed to two relaxation processes with distinct time scales, linked to trap-assisted monomolecular recombination and bimolecular recombination [31]. They also observed that changes induced in the device admittance by small magnetic fields are similar to the changes promoted by small variations in the bias voltage at zero magnetic field, which were attributed to changes in the carrier concentration [31,32]. In this work the effect of temperature was not investigated. As a matter of fact it is known that the OMAR effect generally presents a weak temperature dependence [33], however changes in this parameter could disturb spin dependent mechanisms with specific response times, providing additional information in the frequency domain.

In this report, the effect of a static magnetic field in the electrical impedance was measured in Alq_3-based OLEDs as a function of temperature. Changes on the real and imaginary components of the impedance and capacitance were observed. Simulations employing equivalent circuits and small signal analysis via numerical solutions of Boltzmann transport equations in the drift-diffusion approximation were employed. The results suggest that the MFEs are responsible for (at least) two distinct phenomena on the AC electrical response of the device: *i)* changes on the carrier mobility (in particular an increased hole mobility) that lead to an increase in the current and *ii)* quenching in the bimolecular recombination rate and/or an increase on the minority carrier mobility that lead to an intensification of the negative capacitance effect at low frequencies. It was also observed that the magnetic field induced changes do not present a strong dependence on temperature. The results were interpreted in terms of current models for OMAR.

2. Methodology

2.1. Experimental section

The organic light emitting diode was prepared by thermal evaporation under high vacuum ($< 5 \times 10^{-7} mbar$). All processing outside the vacuum chamber were performed inside an inert gas glove box. Indium tin oxide (ITO) coated glass substrates were cleaned in a sequence of ultrasonic baths using: ethanol, acetone, detergent and Milli-Q water, respectively. The organic layers were deposited as follows: *(i)* $12nm$ thick copper phthalocyanine (CuPc) layer (to improve hole injection); *(ii)* $40nm$ thick N,N′-Di(1-naphthyl)-N,N′-diphenyl-(1,1′-biphenyl)-4,4′-diamine (α-NPD) (as a hole transporting layer - HTL) and *(iii)* $60nm$ thick Alq_3 (electron transporting and emissive layer - ETL). For the top electrode a $0.8nm$ thick LiF layer was deposited followed by a $100nm$ thick Al layer. In order to avoid oxidation processes the device was electrically connected and sealed within a quartz tube with diameter $5mm$ typically employed in electron spin resonance (ESR) experiments.

Electrical impedance spectroscopy (EIS) was measured in a homemade apparatus. The device was subjected to a DC bias voltage (typically $V^{DC} = 3.5V$) superimposed with a small AC voltage with an amplitude of $V_{pp}^{AC} = 100mV$ (peak-to-peak) and in the frequency range $10Hz - 200kHz$. In-phase and quadrature components of the AC current were detected using phase sensitive techniques via a Lock-in amplifier. The magnetic field was generated in a *X* band ESR spectrometer (MiniScope MS300 - Magnettech). The temperature control was performed with the aid of the cryogenic system of the ESR spectrometer.

The experimental frame was composed of 21 consecutively collected electrical impedance spectra (each one comprising the entire frequency range: 10–200kHz, see Fig. 2a). The 21 spectra were collected by alternating the magnetic field applied on the sample between $H_0 = 5.5mT$ and $H_1 = 450mT$ (minimum and maximum values of the employed apparatus). By employing a non zero H_0 we intend to avoid ultra-small magnetic field effects at the same time that we keep the external magnetic field at the same order of typical molecular fields (hyperfine interactions) [33].

EIS were measured at different temperatures, ranging from 233 to $333K$; the DC bias voltage for each temperature was adjusted in order to fix the DC current at $35\mu A$ (with this we always kept the emitting state of the device). During the experiments the DC voltage and temperature were held constant. In all measurements the applied magnetic field was perpendicular to the device substrate.

Since the electric current of these devices typically presents temporal variations, the analysis of the MFEs in electrical response of the device was determined by averaging the differences between the spectra obtained for H_0 (named herein as low field condition - LFC) and H_1 for the entire frequency spectra. For this purpose, linear interpolations were performed for each frequency by considering H_0 and H_1 points separately. The changes induced on the real ($\Delta Z'(f)$) and imaginary ($\Delta Z''(f)$) components of impedance were calculated by subtracting each collected point and the intermediary interpolated value. The average MFE on the impedance were then estimated for each frequency based on 21 values of $\Delta Z'$ and $\Delta Z''$ (see Supplementary Material for an illustrative representation).

The performance of the device was evaluated via JxV curve and voltage dependent optical power emission. Complementary studies on the MFEs induced on device electroluminescence were also performed (see Supplementary Material).

2.2. Simulations

2.2.1. Drift-diffusion approach

In order to assess more information regarding the microscopic mechanisms associated with the MFEs in our system, small signal analyses were performed for a simplified unidimensional bipolar monolayer device via the Drift-Diffusion approach (SSA/DD). Fig. 1 highlights the differences between the real and simplified model device employed in the simulations.

Eqs. (1)–(3) present the relations employed in both steady state

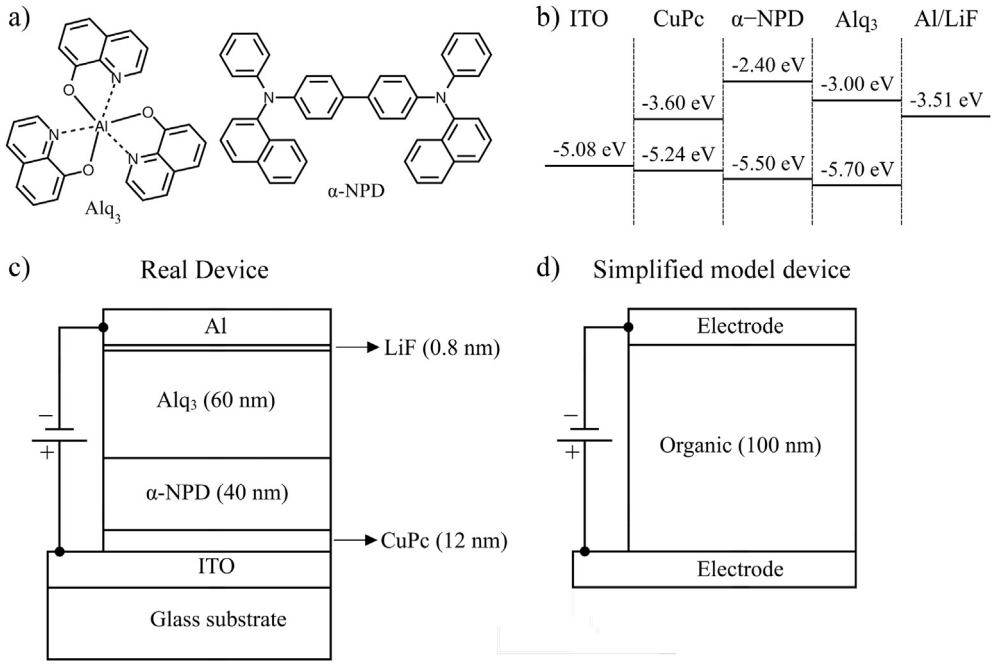

Fig. 1. *a)* Chemical structure of the main constituting molecules of the OLED, and *b)* energy-level alignments associated to the layers. Architecture of *c)* real device and *d)* simplified model device employed in SSA/DD simulations.

and SSA/DD studies of the device:

$$F_\psi(\psi(x),n(x),p(x)) = \varepsilon\frac{d^2}{dx^2}\psi(x) - q[n(x)-p(x)] \tag{1}$$

$$F_n(\psi(x),n(x),p(x)) = \frac{1}{q}\frac{d}{dx}J_n(x) - R(n(x),p(x)) \tag{2}$$

$$F_p(\psi(x),n(x),p(x)) = -\frac{1}{q}\frac{d}{dx}J_p(x) - R(n(x),p(x)) \tag{3}$$

where ε represents the dielectric constant of the organic layer, q is the elementary charge; $\psi(x)$ represents the electric potential distribution inside the device (at x position); $n(x)$ and $p(x)$ represent the density of free electrons and holes. J_n and J_p represent, respectively, the electron and hole current densities given by:

$$J_n(x) = -q\mu_n(x)n(x)\frac{d}{dx}\psi(x) + qD_n(x)\frac{d}{dx}n(x) \tag{4}$$

$$J_p(x) = -q\mu_p(x)p(x)\frac{d}{dx}\psi(x) - qD_p(x)\frac{d}{dx}p(x) \tag{5}$$

The diffusion coefficient (D) was described by Einstein relation [34,35]:

$$D_k(x) = \frac{k_BT}{q}\mu_k(x), \tag{6}$$

and a Poole-Frenkel behavior of charge carriers mobilities (μ) was considered for electrons and holes [36]:

$$\mu_k(x) = \mu_k^0 exp\left(\sqrt{\frac{E(x)}{E_k^0}}\right). \tag{7}$$

where k_BT represents the thermal energy (taken as 0.025 eV), $E(x)$ represents the electric field inside the device at x position, E_k^0 a constant factor (considered as 7×10^5 V/m), and μ_k^0 represents the field independent carrier mobility coefficient.

The recombination was described via Langevin equation [37]:

$$R(n(x),p(x)) = R_L\frac{q}{\varepsilon}\left[\mu_n(x)+\mu_p(x)\right]n(x)p(x) \tag{8}$$

where R_L is a pre-factor, initially considered as 1.

Steady state conditions were set up by considering $F_\psi(\psi,n,p)=0$, $F_n(\psi,n,p)=0$ and $F_p(\psi,n,p)=0$ in Eqs. (1)–(3). Scharfetter-Gummel approach was employed for the discretization of the current densities [38]. The boundary conditions $\psi_1=0$ and $\psi_N = V_{appl}-V_b$ were employed for the potentials; where V_{appl} represents the applied voltage and V_b the internal built-in voltage. The charge densities at the vicinities of the electrodes were calculated by using Gauss-Fermi integrals involving the estimated frontier energy levels of the organic materials (E_{HOMO} and E_{LUMO}), the work function of the electrodes (W_{anode} and $W_{cathode}$) and a Gaussian density of states (with $\sigma_{HOMO}=\sigma_{LUMO}=0.1eV$). The charge injection was performed by considering an effective injection barrier of $\varphi_p(\varphi_n) = E_{HOMO}(E_{LUMO}) - W_{anode}(W_{cathode})$ [39]. Initial steady state solutions were iteratively obtained via Gummel method and refined via Newton method.

SSAs were performed by setting $F_\psi(\psi,n,p)=0$, $F_n(\psi,n,p)=dn/dt$ and $F_p(\psi,n,p)=dp/dt$ in Eqs. (1)–(3). The time dependent response of the system was calculated by the linearization around the stationary solutions (ψ_0,n_0,p_0) of Eqs. (1)–(3) subjected to a small perturbation [40]:

$$(\psi(t),n(t),p(t))^T = \left(\psi^0,n^0,p^0\right)^T + \left(\psi^{AC},n^{AC},p^{AC}\right)^T\cdot e^{i\omega t} \tag{9}$$

Expanding the DD equations around $F_\psi(\psi_0,n_0,p_0)=F_\psi^{DC}=0$, $F_n(\psi_0,n_0,p_0)=F_n^{DC}=0$ and $F_p(\psi_0,n_0,p_0)=F_p^{DC}=0$ the resulting system of equations was solved by:

$$\left(\begin{bmatrix} \frac{\partial F_\psi}{\partial \psi} & \frac{\partial F_\psi}{\partial n} & \frac{\partial F_\psi}{\partial p} \\ \frac{\partial F_n}{\partial \psi} & \frac{\partial F_n}{\partial n} & \frac{\partial F_n}{\partial p} \\ \frac{\partial F_p}{\partial \psi} & \frac{\partial F_p}{\partial n} & \frac{\partial F_p}{\partial p} \end{bmatrix} - i\omega \begin{bmatrix} 0 & 0 & 0 \\ 0 & I & 0 \\ 0 & 0 & I \end{bmatrix} \right) \begin{pmatrix} \psi^{AC} \\ n^{AC} \\ p^{AC} \end{pmatrix} = \begin{pmatrix} 0 \\ 0 \\ 0 \end{pmatrix} \quad (10)$$

where F_k, ψ^{AC}, n^{AC}, p^{AC} represent vectors whose components are associated with $N-2$ discretized sites, excepting the boundary conditions set as $\psi_1^{AC} = \psi_N^{AC} = n_1^{AC} = n_N^{AC} = p_1^{AC} = p_N^{AC} = 0$.

After obtaining J_n^{AC} and J_p^{AC}, the displacement current $J_d^{AC} = \varepsilon.(\partial E^{AC}/\partial t)$ (where E^{AC} is the AC electric field on the device) was added to obtain the total current density of the device $J_t^{AC} = J_n^{AC} + J_p^{AC} + J_d^{AC}$.

The influence of the external magnetic field was incorporated in the model by considering small changes induced on μ_n^0, μ_p^0 (Eq. (7)), R_L (Eq. (8)), φ_n and φ_p parameters. These changes are consistent with most of the MFEs predicted by the currently accepted OMAR models [16–24]. Such effects were incorporated in the model by performing small percentual changes on the initial parameters set (employed to simulate the impedance and capacitance spectra at LFC) and comparing the resulting changes with those experimentally observed. It is important to highlight that such approach is just possible because the experiment was conducted by considering a constant influence of the magnetic field on the electrical response of the device. Modulated magnetic perturbations would require more sophisticated approaches [28,30].

2.2.2. Equivalent circuit approach

Complementary equivalent circuit (EC) analyses were also performed to evaluate the AC response of the OLED. For this purpose the system was simulated by considering a parallel RC circuit in such a way that the real ($Z'(f)$) and imaginary ($Z''(f)$) components of the impedance were described by Eq. (11).

$$Z(f) = Z'(f) + Z''(f)i = \frac{R}{1+(2\pi f R C)^2} - \frac{2\pi f R^2 C}{1+(2\pi f R C)^2} \cdot i \quad (11)$$

The influence of the external magnetic field was incorporated in the system by performing small percentual changes on the total resistance (R) and capacitance (C) of the system (i.e. $X_1 = X_0 + \alpha X_0$, for $X = R$ or C).

The frequency dependent resistance ($R(f)$) and capacitance ($C(f)$) were estimated via Eq. (11) by:

$$C(f) = Im\left[\frac{1}{2\pi f Z(f)}\right] \quad (12)$$

$$R(f) = \frac{1}{Re[1/Z(f)]} \quad (13)$$

3. Results and discussions

3.1. Experimental

Fig. 2 shows a typical impedance spectra obtained at LFC (normalized in relation to $Z'(10Hz)$) and the respective capacitance spectrum (normalized in relation to the geometric capacitance, C_{geo}). Full circles represent the experimental data points, open circles represent the curves coming from EC fitting and the full lines from SSA/DD simulations (see Section 3.2 for details).

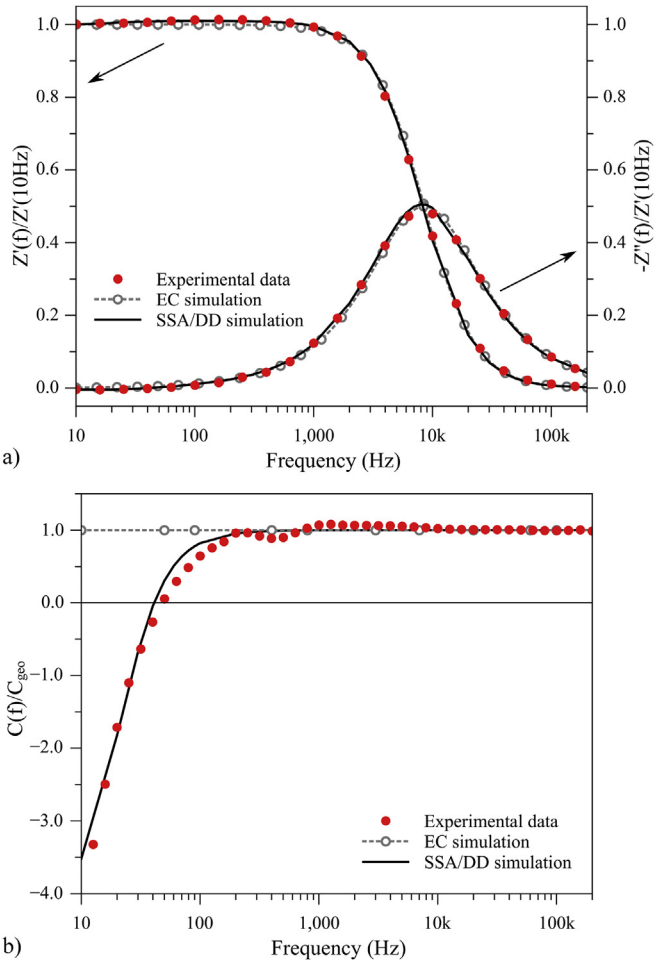

Fig. 2. Experimental (full circles) and simulated curves obtained via EC (open circles) and SSA/DD (full lines) approaches for Alq_3-based OLED at 293K and $H_0 = 5.5mT$ (LFC). *a)* Real (Z') and the negative of the imaginary ($-Z''$) components of the standardized impedance spectra (taken in relation to Z' at 10Hz, i.e. $Z'(f)/Z'(10Hz)$ and $Z''(f)/Z'(10Hz)$), and *b)* normalized capacitance spectra (based on geometric capacitance, $C_{geo} = 1.35nF$).

As evidenced in Fig. 2b, the effect of negative capacitance (NC) is observed for frequencies below 30Hz. This phenomenon is commonly reported for OLEDs, being mainly associated with the dynamics of the charge carriers in the device and space charge [30,41]. In general NC is more pronounced at low frequencies, where the response times of the charge carriers (mainly the less mobile ones) are of the same order of the external AC excitation (see Ref. [41] for details).

Fig. 3 illustrates the changes induced by the magnetic field on the capacitance and resistance spectra of the device, obtained via Eqs. (12) and (13). The percentual changes of the parameters $R(f)$ and $C(f)$ were calculated in relation to the resistance at 10Hz ($R_{ref} = R(10Hz)$) and the geometric capacitance ($C_{ref} = C_{geo}$), both at the LFC ($\Delta X(f) = X_1(f) - X_0(f)/X_{ref}$, where X_i represents the parameter X in the presence of the field H_i, for $X = R$ and C).

In general it is observed that the external magnetic field induces a reduction on both parameters, $C(f)$ and $R(f)$. For the capacitance, the major changes are observed at low frequencies (up to −20%), at the same region where NC effects are noticed (see Fig. 2b), intensifying it. On the other hand, a constant change on the device resistance is observed for the whole spectra (around −1%).

Similar changes in $C(f)$ have been reported by Djidjou et al. and attributed to changes induced on the trap-assisted and bimolecular

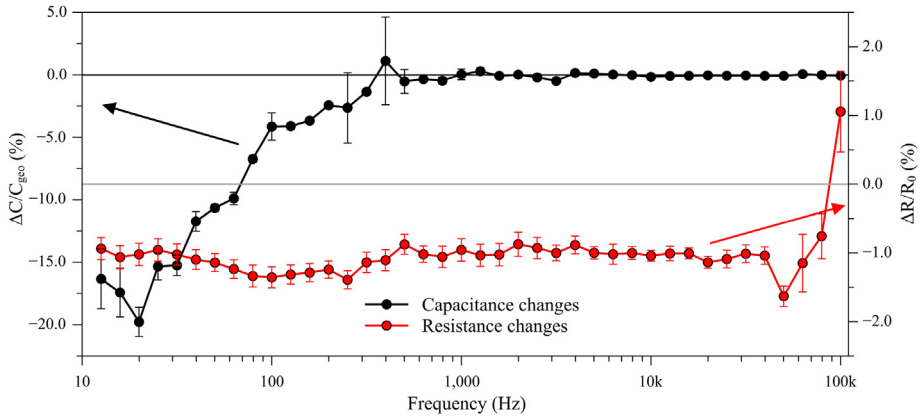

Fig. 3. Frequency dependent changes induced on the capacitance (black) and resistance (red) spectra of the device by the external magnetic field. (For interpretation of the references to colour in this figure legend, the reader is referred to the web version of this article.)

recombinations [31,32]. The changes observed in the resistance are compatible with previous results reported by Gómez et al. for a similar device [42].

Fig. 4 illustrates the average changes induced by the external magnetic field on the real and imaginary components of the impedance spectra. The continuous lines show the adjusted curves for $\Delta Z'$ $(Z'_1 - Z'_0)$ and $\Delta Z''$ $(Z''_1 - Z''_0)$ obtained via EC approach (discussed in Section 3.2).

Note that the magnetic field induces a quenching in Z' for frequencies below $7kHz$, while an emergent asymmetric peak is observed for $\Delta Z''$ (which is not at the same position of Z'' peak shown in Fig. 2a). At first these results suggest that the magnetic field influences the electrical response of the device on a broader frequency range. Note that the lineshapes can be associated to Kramers-Kronig relation [43].

Fig. 5 shows EIS and capacitance spectra acquired at different temperatures: 233, 273, 293, 313 and $333K$. In these experiments the DC current densities were kept constant in the device (by appropriate adjustment on the applied voltage) in order to minimize any influence of changes in the carriers mobility (see Supplementary Material).

As can be seen a decrease in the amplitude of the real and imaginary components of the impedance spectra is observed with increasing temperature, which means that the OLED becomes less resistive as expected. It is also observed a shift of the Z'' peak towards higher frequencies (f_p) for higher temperatures, which evidences small changes on the carrier mobilities [44]. By contrast, $C(f)$ has a similar trend independent of the temperature, especially at low frequencies; some systematic dependence is observed at intermediate frequencies (from $200Hz$ to $20kHz$).

Regarding the MFEs, the same pattern for $\Delta Z'$ and $\Delta Z''$ are observed, independently of the temperature used. In general ΔC presents the same trends at different temperatures. For ΔZ, some systematic changes can be observed only for the parameter f_c (the cutoff frequency, for which $\Delta Z'(f_c) = 0$) which are compatible with the changes observed in f_p (the frequency associated with the Z'' peak position for EIS at LFC) highlighted in Fig. 5. Indeed, as can be seen in the inset of Fig. 5c, these parameters present a similar dependence with temperature, which suggest that the changes induced in f_c and f_p have the same origin, and can be associated with small changes on carrier mobilities on temperature. This hypothesis is reinforced by preliminary SSA/DD simulations performed by supposing a temperature dependence on charge injection (Fermi-Gauss integral) and carrier mobilities $(\mu_k^0 = \mu_k^0(T))$ [36] (not shown here for simplicity). Given these considerations, we can conclude that the observed MFEs have a very weak temperature dependence, at least in the current density employed.

As a matter of fact Bagnich et al. have shown that MFEs can present different temperature dependences depending on the current density, which was attributed to electron-hole pairs lifetimes [45]. In particular it was shown that it is possible to observe a very weak temperature dependence in a wide current density range, which is compatible with the results presented in Fig. 5.

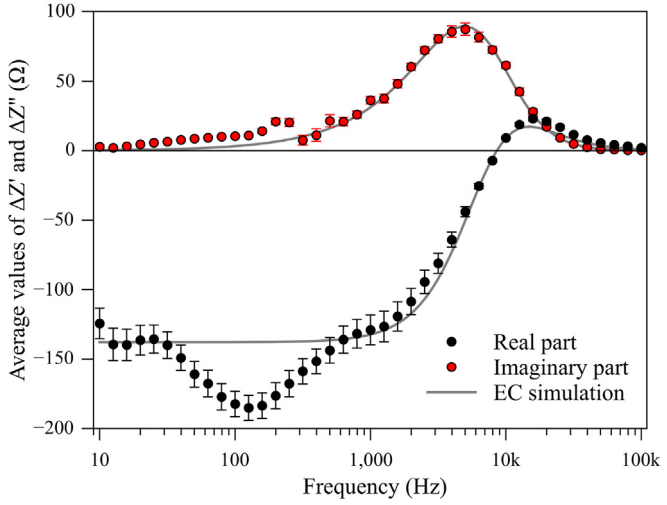

Fig. 4. Average values of $\Delta Z'$ and $\Delta Z''$ induced by MFE on the device at $293K$. Circles represent the experimental data and continuous lines represent the curves estimated via EC simulation.

3.2. Simulations

Given the number of static and dynamic variables involved in the charge transport/recombination and their interdependence, it is very difficult to underline the exact mechanism associated with the observed MFEs in the device AC response. In order to interpret the results, simulations employing EC and SSA/DD approaches were carried out.

For this purpose an initial optimization of parameters was performed in order to reproduce the typical spectra presented in Fig. 2. For EC simulation $R_0 = 13.78 \pm 0.08k\Omega$ and $C_0 = 1.35 \pm 0.01nF$ had provided the best agreement. Table 1 presents the set of parameters employed in the SSA/DD approach.

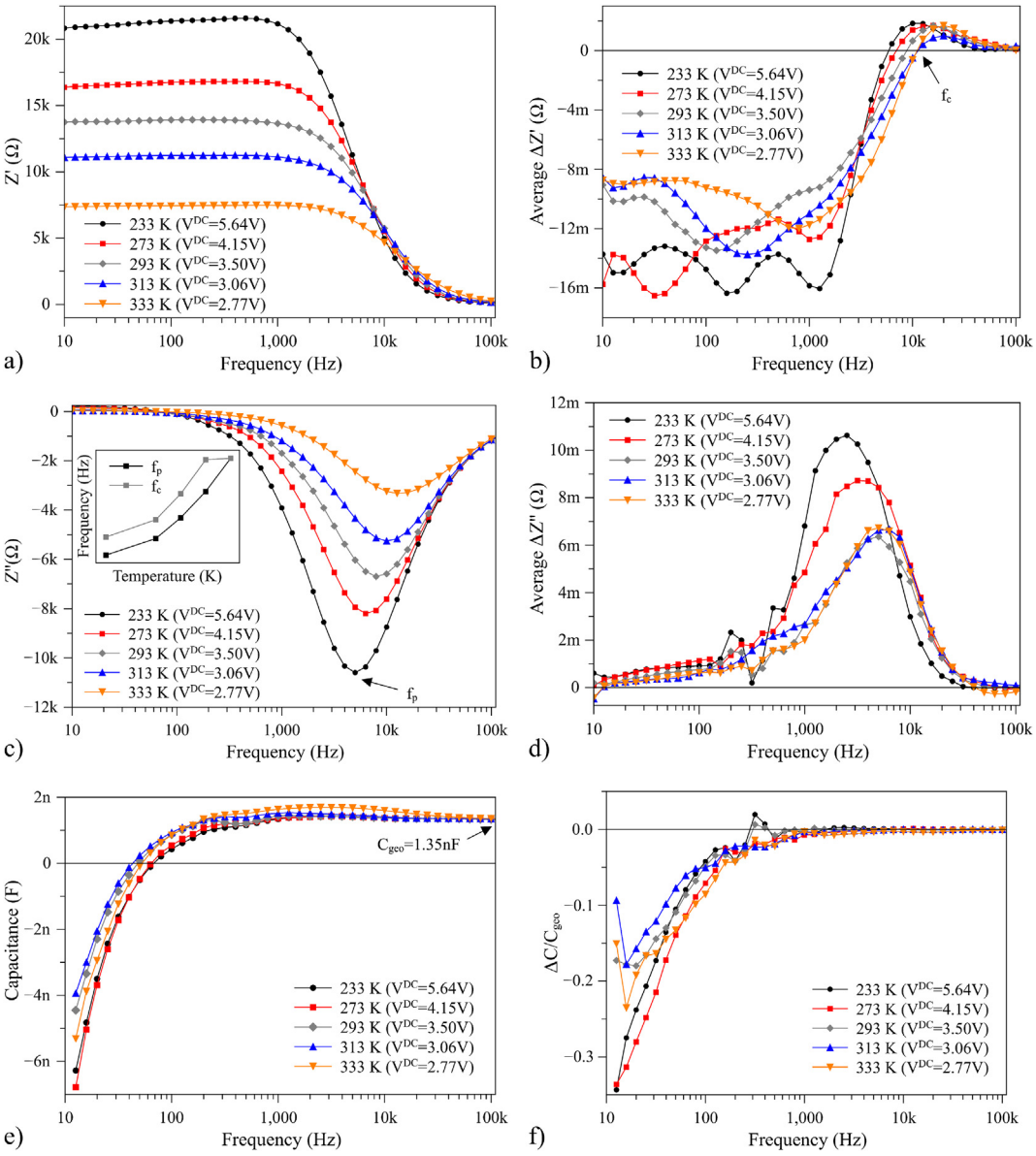

Fig. 5. Impedance spectra, capacitance spectra and associated MFEs at distinct temperatures (*a*), *c*) and *e*) curves were acquired at LFC).

Table 1
Physical parameters that better represent a real device, reported by Tutiš et al. [46] and the adjusted values employed in our simplified model device.

Parameters	Real multilayer device [46]		Simplified model device	
Work function (eV)	ITO/CuPc	−5.24	W_{anode}	−5.45
	Al/LiF	−3.51	W_{catode}	−3.26
E_{HOMO} (eV)	α-NPD	−5.50	Organic layer	−5.80
	Alq_3	−5.70		
E_{LUMO} (eV)	Alq_3	−3.00	Organic layer	−3.00
μ_p (m^2/Vs)	α-NPD	10^{-9}	Organic layer	3.88×10^{-11}
	Alq_3	10^{-13}		
μ_n (m^2/Vs)	Alq_3	10^{-12}	Organic layer	1.08×10^{-15}

SSA/DD parameters were obtained from a systematic study by initially considering some optimized parameters reported for a similar device [46]. It is interesting to note that despite of the model simplicity, in general the optimized values were not so dissonant from those expected for real devices, excepting for μ_n. In the present case, the large deviation associated with this parameter can be associated with the presence of interfaces in the organic layer of the real device, where negative charges are supposed to accumulate during the device operation [46]. Such feature, associated with the lower mobility of electrons expected in α-NPD (trap limited transport [47]) could indeed lead to the reduced mobility obtained in our model device.

Nevertheless it is important to stress here that, given the simplicity of the employed model, the main objective of the SSA/DD simulations is not establishing a reasonable set of parameters for device simulation or even provide precise curve fittings, but only evaluate the main role of MFEs on some device descriptors in order to identify which are associated with the observed responses. Additional studies considering the interfaces (and exciton dynamics) are necessary for a more in-depth analysis.

As can be noticed in Fig. 2, the electrical behavior of the device is well described by a simple EC simulation in a wide frequency range. Large deviations are observed in the capacitance spectra at low frequencies ($f < 100Hz$), just where the NC phenomenon starts (and

then the use of a pure RC system is no longer applicable). On the other hand, despite the simplicity of our monolayer device, the simulation via SSA/DD was able to reproduce the experimental curves, including the NC effect. In this case larger deviations are observed in an intermediary frequency range (between 25 and 100 *Hz*) that can be associated with the trap assisted recombination contribution [31], that is not considered in our simplified model.

For the simulation of $\Delta Z'$ $(Z'_1 - Z'_0)$ and $\Delta Z''$ $(Z''_1 - Z''_0)$ via EC approach (Fig. 4) the variations employed, which are associated with the magnetic field induced changes, were $\Delta R = -0.01R_0$ (-1% of change) and $\Delta C = 0.0$. The good fits obtained indicate that the predominant behavior of $\Delta Z'$ and $\Delta Z''$ curves can be ascribed to a constant variation on the resistance of the device, which is also compatible with $\Delta R/R_0 \sim -1$ % as presented in Fig. 3. Larger deviations are observed below 1 *kHz*, mainly for $\Delta Z'$, where fluctuation are observed around the predicted value (that is also observed for different temperatures, see Fig. 5). In fact, the interpretation of such effect is not simple. Preliminary SSA/DD studies suggest that it could be associated with trap effects, however more studies are necessary.

In order to evaluate the changes promoted in the device response due to small changes on μ_n^0, μ_p^0, R_L, φ_n and φ_p parameters (induced by the static magnetic field), the impedance and capacitance spectra of the model system were simulated considering systematic variations of the values initially associated with the LFC (SSA/DD spectra shown in Fig. 2a–b obtained via the parameters presented in Table 1). Fig. 6 illustrates the influence of each parameter on the impedance and capacitance of the device. The curves were normalized by $Z'_0(10Hz)$ and C_{geo}. For each analysis, just one parameter (X) was changed by a small factor α ($X = (1+\alpha).X_0$), while the others were kept constant (obtained for LFC).

As can be noticed, the modifications on μ_p and φ_p lead to larger changes on the impedance spectra as compared to μ_n, φ_n and R_L. In general, an increase on μ_p^0 ($\alpha = +1.25\%$) or a decrease on φ_p parameter ($\alpha = -0.15\%$) appropriately describes the observed changes on Z' and Z'', however the effects on the capacitance are underestimated for both, with an opposite effect associated with $\Delta\varphi_p$. On the other hand, despite the small effect induced by μ_n and R_L on the impedance spectra, these parameters dominate the changes on device capacitance, which is compatible with the results reported by others [28–32]. In particular, an increase in the electron mobility and a decrease of the Langevin recombination parameter of around 1% can lead to capacitance changes of the same order of that observed in Fig. 3. In general changes in the injection barriers lead to non compatible behaviors for $\Delta Z'$, $\Delta Z''$ and ΔC.

The results presented in Fig. 6 suggest that variations on μ_p, μ_n and R_L are compatible with the MFEs observed in the impedance and capacitance spectra. Fig. 7 illustrates the curves $\Delta Z'$, $\Delta Z''$ and ΔC as a result of the variations concomitantly imposed to these three parameters. An increase for the mobilities and a decrease for the recombination of 1% and 1.25% were considered. Note that for $|\alpha| = 1.25\%$, that provided the best fit for individual changes (Fig. 6), overestimates the overall effect, indicating an expected interdependence of the parameters. The best fit is obtained for $|\alpha| = 1\%$. A similar study was performed by considering concomitant changes on φ_p and R_L parameters (see Supplementary Material).

Such results show that the MFEs observed in our device can be associated (at least) with two concomitant effects: *i)* device resistance reduction, induced by an increase on the mobility of the more mobile carriers, and *ii)* frequency dependent capacitance changes, promoted by an increase on the mobility of the less mobile carrier and/or a reduction on the bimolecular recombination rate.

Regarding the changes on the device capacitance, the reduction of R_L parameter is indeed compatible with the intensification of the NC effect. As a matter of fact, in a series of theoretical studies on NC employing DD equations, Gommans and collaborators [41] have shown that reduced Langevin recombination rates lead to more intense NC effect at low frequencies, similar to that observed in Fig. 3. It is argued that the reduction of the carriers recombination leads to a more significant interpenetration of negative and positive carriers, reducing the effective space charge, and intensifying the NC effects [30,41]. The reduction of R_L is also compatible with the MFEs reported by Li et al. which have attributed the changes on the electroluminescence of a similar Alq_3-based device to a reduction of the bimolecular recombination coefficient [48].

In this context it is important to note that in the framework of the employed DD approach, a reduction in the bimolecular recombination rate can be associated to changes on the free charge density. The precursor pairs associated with the formation of excitons can recombine (leading to the generation of excitonic states) or dissociate at specific rates, and $R(n,p)$ represents the balance between these rates. Thus a reduction in the R_L obtained in our simulation is not in contradiction with the electroluminescence enhancement typically observed in Alq_3 based OLEDs [21,48–50] (as a matter of fact, positive magnetoelectroluminescence effects were also observed in our device, see Supplementary Material).

Finally, the association of MFE with the dynamics of the slowest carrier (called minority carriers in devices with well balanced e-h injection) is also described in the literature [28–30]. In particular, the association of less mobile carriers with ΔC in organic devices is mainly due to the frequency range where this MFE is observed (low frequency domain) that is of the same order of the transit time of these carriers. Indeed, our simulation shows a significant influence of $\Delta\mu_n$ on the intensification of NC effect.

3.3. Considerations regarding the current OMAR models

Despite the above mentioned changes being compatible with our experimental results, it is important to keep in mind that they can in fact be associated with very complex processes, that can not be described by our simple model (such as interaction of accumulated carriers at the interfaces, exciton dynamics, charge-exciton reactions, etc). However it is possible, at least, to underline mechanisms associated with the currently accepted OMAR models that could lead to such concomitant MFEs in the device. In this context, we present below an analysis of our main results based on these models.

Let us start with the bipolaron (BP) model. In this model it is supposed that the external magnetic field decreases the probability of BP formation. If the formation of bipolarons is a relevant intermediate mechanism for charge transport, the net effect induced by the magnetic field is a negative change in the device current by hopping blockage (spin blocking mechanism) [51]. On the other hand, positive changes are expected if BP formation act as an effective trapping mechanism in the device [26,27]. In this context, decreasing BP formation increases the free charges density, increasing the total current [16]. In our device a positive current response is observed, in such a way that BP trap mechanism could be involved, leading to an increase in the carriers density in the transport layers (in particular, given charge accumulation at the organic/organic interface, positive BP can be considered more likely in our device).

In our simulations such effect is well described by the changes promoted in φ_p, specially because interfaces effects or exciton-charge reactions are not relevant to this transport layer. However despite that the changes on impedance are compatible with an increase in the density of holes (decrease in φ_p) the changes in the capacitance are not compatible with the experimental results,

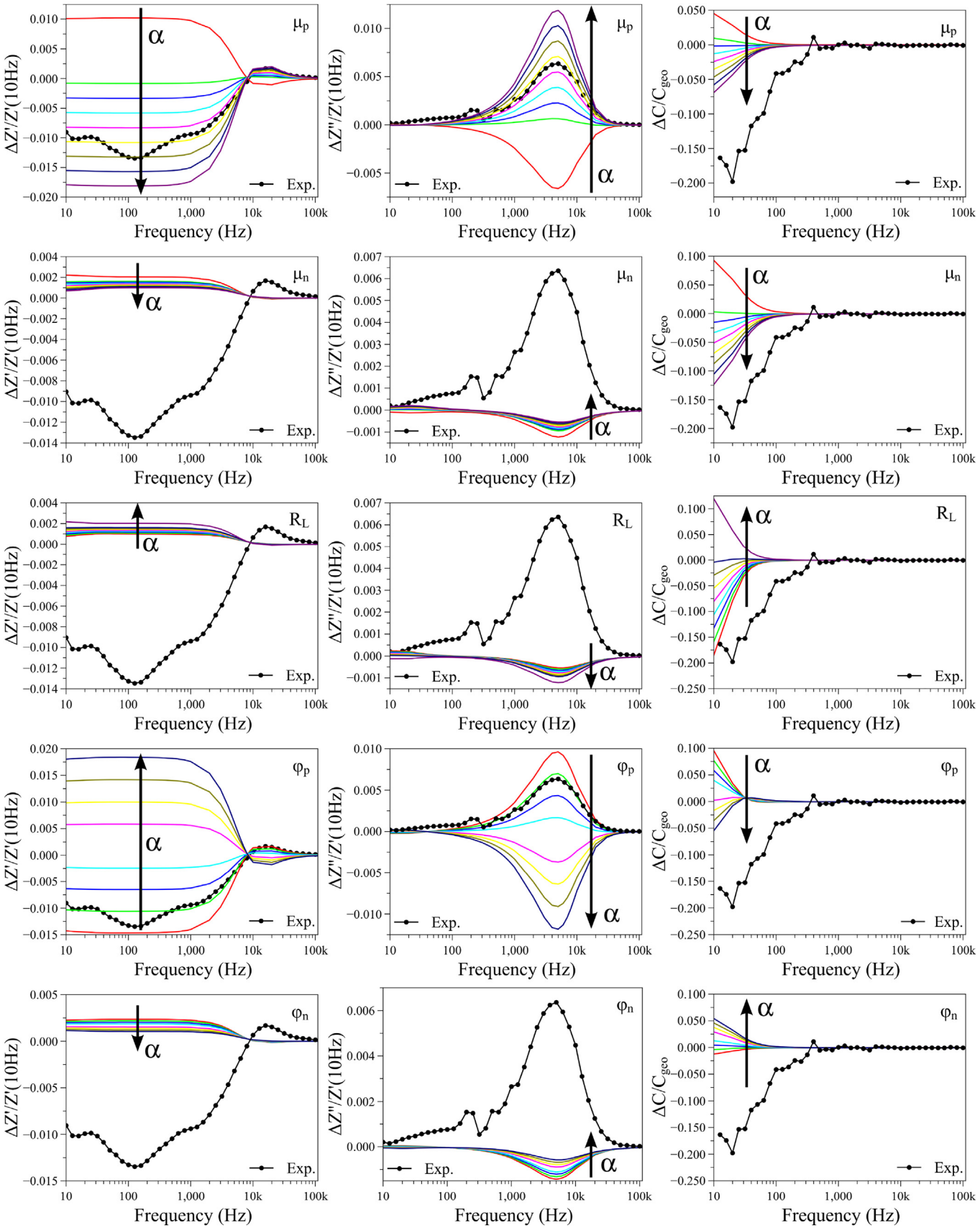

Fig. 6. Systematic study of the changes induced on the standardized $Z'(f)$, $Z''(f)$ and $C(f)$, due to small variations on the parameters: *a)* μ_p^0, *b)* μ_n^0 (for $\alpha\% = -1.00$, 0.25, 0.50, 0.75, 1.00, 1.25, 1.50, 1.75, and 2.00), *c)* R_L (for $\alpha\% = -2.00$, -1.75, -1.50, -1.25, -1.00, -0.75, -0.50, -0.25, and 1.00), *d)* φ_p and *e)* φ_n (for $\alpha\% = -0.20$, -0.15, -0.10, -0.05, 0.05, 0.10, 0.15, and 0.20). The arrows indicate the effect promoted by an increase in $\alpha\%$ parameter.

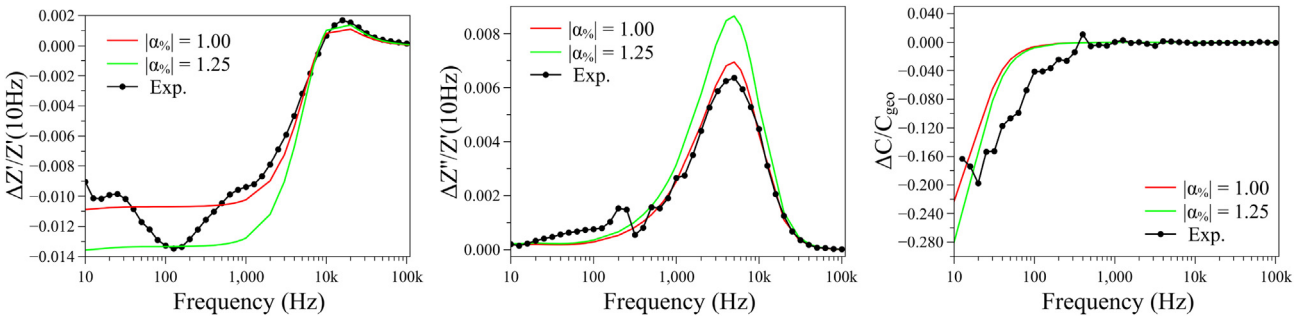

Fig. 7. The best fit obtained for the standardized $\Delta Z'(f)$, $\Delta Z''(f)$ and $\Delta C(f)$ via SSA/DD approach. Concomitant changes on the parameters μ_p^0, μ_n^0, and R_L were considered: *i)* $|\alpha| = 1.00\%$ (red lines) and *ii)* $|\alpha| = 1.25\%$ (green lines). (For interpretation of the references to colour in this figure legend, the reader is referred to the web version of this article.)

which undermines this hypothesis.

However, the crucial problem of the BP model to interpret our results is the explanation of magnetic field induced changes on the recombination rate. For this purpose it should be necessary to consider a mechanism in which a reduction in the BP population could lead to changes in the recombination. In this context, the suppression of bipolaron/polaron (BP/P) reactions could be an alternative.

Interestingly such mechanism is often disregarded in the explanation of OMAR, in spite of its known influence on electroluminescence [52–54]. In general, BP/P reactions involve different microscopic mechanisms, but the net effect can be described by Eq. (14) [53].

$$BP^{++(--)} + P^{-(+)} \rightarrow h\nu + P^{+(-)}. \tag{14}$$

Bipolarons are generally formed in the singlet configuration, so BP/P reactions can be considered a spin-independent process, though BP generation is a spin dependent event [55]. This and the higher Coulomb interaction among the involved species, turn the BP/P reactions more efficient than $P^{+(-)}/P^{-(+)}$ ones, so that a reduction of BP population could lead to a quenching in the effective recombination. Nevertheless BP/P reactions are not plausible in our case. Considering charge accumulation [46], such mechanisms should be more relevant at the electron and hole transport layers (ETL and HTL) interface. In our device it is expected to involve positive BP (BP^{++}) and electrons (P^{-}), so an effective BP/P reaction supposes a hopping of BP^{++} into the emissive layer, which is not a probable mechanism, given the energy level alignments of Alq_3 and α-NPD frontier orbitals [46] as well as the low mobility expected for this specie. We believe, however, that the plausibility of such mechanisms deserves more detailed studies.

In this context, double-carrier mechanisms, such as the ones involving electron-hole pair (e-h pair) and triplet/polaron reaction (TPR), provide a more direct interpretation of our data. In the e-h pair model it is supposed that electrons and holes form correlated pairs (called e-h pairs) during the charge transport process, which despite being coulombically (weakly) bound are far enough from each other so that the exchange effects are negligible compared to the hyperfine interactions. The e-h pairs are supposed to recombine, forming singlet (S) or triplet ($T_{+1,0,-1}$) excitons, or dissociate back into free charge carriers with specific rates. The model predicts that an external magnetic field can change the population of S and T precursor pairs in the device, modifying the balance of singlet and triplet excitons at steady state, and consequently the electrical and optical responses. The net effect depends on the intrinsic transition rates associated with S and T e-h lifetimes, τ_r^S and τ_r^T (that lead to the formation of S and T excitons), as well as their respective dissociation rates (k_d^S and k_d^T). In particular Bagnich et al. in their study about the MFE on PPV-based devices demonstrated that an enhancement of the device current (compatible with a reduction in the resistance) and electroluminescence (typically also observed in Alq_3 based OLEDs, see Supplementary Material) could be obtained by considering $\tau_r^S/\tau_r^T > 1$ and $k_d^T/k_d^S \leq 1$ which suggest that S e-h pairs have a longer lifetime and higher dissociation rate than T [45].

Indeed, positive MFEs in electroluminescence have been observed for Alq_3-based OLEDs, suggesting that the magnetic field leads to an enhancement of S population in these devices [21,48–50]. By considering that $k_d^T/k_d^S \leq 1$, which is compatible with the proposition of Hu and collaborators that singlet e-h pairs are more easily dissociated than triplet ones, given the more ionic nature of the wave function associated to them [23], the increase in the S e-h pairs can reduce the effective formation of excitons (despite of increasing the proportion of S:T excitons), leading to an effective reduction in the bimolecular recombination rate, that is compatible with the reduction of the R_L parameter in our simulations. Additionally, as already stated, it leads to a higher interpenetration of positive and negative charges, leading to a intensification of the NC effect.

However it is difficult to interpret changes in the charge carriers mobilities via the e-h pair model. In this model, positive magnetoconductance is generally associated with the current coming from pair dissociation [17] or release of trapped charges induced by T excitons [24]. In our simulations, pair dissociation is already considered in R_L changes and it is not able to reproduce the experimental results. On the other hand, an increase in T population that could lead to significant release of trapped charges is not compatible with positive MFE in electroluminescence (at least in conjunction with the $k_d^T/k_d^S \leq 1$ condition).

Let us consider the TPR model. This model was initially proposed by Desai et al. and states that a large number of T excitons is present in OLEDs under steady state condition (since they present a long lifetime compared to S excitons), which diffuse through the organic material. It is claimed that such T excitons could interact with free carriers (P) according to the following mechanism [21]:

$$T + P \underset{}{\overset{k_1}{\longleftrightarrow}} (T\cdots P) \xrightarrow{k_2} P + S_0^* \tag{15}$$

where $(T\cdots P)$ represents an intermediate state and S_0^* represents an excited vibrational level of the molecule ground state. The first term of Eq. (15) represents the free charge scattering by a triplet exciton, which is assumed to promote a decrease in the carrier mobility. The last one represents the triplet-polaron quenching effect associated with non-radiative decay of T excitons.

According to the TPR mechanism, the external magnetic field changes the interconversion between S and T excitonic states, leading to a decrease in the T excitons population. Such an effect reduces the probability of triplet-charge reactions, leading to a

reduction of scattering processes and, consequently, to an effective increase on the carrier mobilities. By increasing the S exciton population, it also leads to positive changes on the device electroluminescence.

Thus, the TPR mechanism can explain the increase in the carriers mobility, but not the changes on R_L. TPR involves the interconversion between excited neutral states (T and S excitons), that are in principle monomolecular species, so this mechanism is not supposed to induce changes on the bimolecular recombination rate $R(n,p)$. In this context, an interesting question is: If Eq. (15) represents a plausible mechanism associated to the T excitons dynamics, the reduction of T e-h pairs (and consequently T excitons) proposed in the e-h pair model could not lead to the same quenching in the scattering processes proposed in the TPR mechanism? Or, in other words, could the e-h pair mechanism be associated to the carrier mobility enhancement induced by TPR quenching?

As a matter of fact, in the framework of the double-carrier mechanisms, Hu et al. describe the role of TPR in a distinct way, where scattering effects are not (explicitly) considered [23,56]. On the other hand, recently Cox et al. proposed that trions could be considered as one of the causes of OMAR, whose main effect is compatible with carriers scattering via TPR mechanism [57]. So that the real role of TPR in OMAR is not well defined.

In a relatively recent work Peng et al. have suggested that TPR is not the dominant mechanism for the MFE in Alq_3-based OLEDs [50]. Transient electroluminescence experiments were performed in an ITO/NPB/Alq_3/LiF/Al device and no difference on delay time (t_d) between the application of the pulse voltage and the intersection of the rising edge of the pulse EL signal was observed for different offsets and pulse voltages. Since the formation of triplet excitons should be expected due to the applied voltage offset, it was proposed that the TPR could not be associated to significant changes on the carrier mobilities. However, the interpretation of transient spectra of multilayer devices is quite complex, and encompasses charge accumulation effects as well a variety of interactions that turns the t_d interpretation difficult. In particular, for the electric field range considered in Ref. [50], Barth et al. have already pointed out that t_d is associated with holes accumulation at organic/organic interface rather than charge carriers transport [58], undermining its direct association to MFEs that are supposed to occur in the Alq_3 layer. In this context, the results reported by Peng et al. can be better associated to the absence of the BP mechanisms, since these species are more likely present close to the interface (in particular HTL, due to the high hole density at the organic/organic interface [46]).

Dark injection (DI) experiments can provide more reliable data and are easier to interpret. In this context, Song et al. have shown that TPR can induce changes on the carrier mobilities in N,N′-diphenyl-N,N′-bis(3-methylphenyl)-(1,1′-biphenyl)-4,4′-diamine (TPD), attesting the significant influence of TPR in OMAR effect [59].

Given this scenario, TPR can indeed be considered a relevant mechanism associated to MFE in organic devices. Once its influence is associated with changes induced on the T excitons density, and considering that it depends on the population of T e-h precursor pairs, we consider that it can be easily evaluated using e-h pair models, such as the ones proposed in this work. In this sense, we can conclude that the observed MFEs in our device can be directly understood in terms of e-h pairs interconversion which leads to an increased S e-h pairs population. Such effect, in turns, promotes: *i)* an enhancement of S exciton population, leading to a positive change in the device electroluminescence (see Supplementary Material); *ii)* a higher interpenetration of positive and negative charges, since S e-h pairs present a more pronounced dissociation rate, that leads to an intensification of NC effect and reduced bimolecular recombination rate; and *iii)* a decrease in the T exciton population that leads to a reduction of free charges scattering, which leads to an increase in charge mobility and positive magnetoconductance. In this framework the changes induced on the current density and electroluminescence have the same origin.

In fact, distinct and more complex scenarios could be speculated, since the presence of organic/organic interfaces in the device could change the interdependence between charge mobilities and recombination rates. In this context, more sophisticated simulation models including interfaces, charge accumulation and exciton dynamics could provide a more detailed picture, however it is out of the scope of this paper.

4. Conclusions

Electrical impedance spectroscopy measurements were performed in the presence of external magnetic fields on Alq_3-based OLED at different temperatures. Magnetic field effects were observed on the impedance and capacitance spectra of the device. Changes of up to 20% have been observed on the capacitance spectra at low frequencies (below 100*Hz*), while smaller variations were identified on the real and imaginary components of the impedance spectra. The results showed that the involved MFEs do not present a strong temperature dependence. Simulations employing SSA/DD approach (on a simplified device model) and RC equivalent circuits suggest that the observed electrical changes (induced by an external DC magnetic field) can be associated with an enhancement of the carriers mobility and a quenching of the recombination rates, that leads to a reduced resistance and a more intense NC effect in the device. The results were interpreted in terms of the currently accepted OMAR models and the best agreement was with the so called e-h pair model. Given the magnitude of the changes observed in the impedance and capacitance of the device, our results also suggest that OMAR effect can be employed for the development of magnetic-field dependent low-pass filters.

Acknowledgements

This work was financially supported by Fundação de Amparo à Pesquisa do Estado de São Paulo (FAPESP) (proc. 2012/03116-7, 2011/21830-6 and 2008/57872-1 INCTMN), CNPq (proc. 448310/2014-7) and CAPES (proc. 1804-12-0, 23038.008351/2010-17).

Appendix A. Supplementary data

Supplementary data related to this article can be found at http://dx.doi.org/10.1016/j.orgel.2017.08.003.

References

[1] J.L. Martin, J.D. Bergeson, V.N. Prigodin, A.J. Epstein, Magnetoresistance for organic semiconductors: small molecule, oligomer, conjugated polymer, and non-conjugated polymer, Synth. Met. 160 (3–4) (2010) 291–296, http://dx.doi.org/10.1016/j.synthmet.2010.01.009.

[2] G. Veeraraghavan, T.D. Nguyen, Y. Sheng, O. Mermer, M. Wohlgenannt, An 8×8 pixel array pen-input oled screen based on organic magnetoresistance, IEEE Trans. Electron Devices 54 (6) (2007) 1571–1577, http://dx.doi.org/10.1109/TED.2007.895240.

[3] M. Wohlgenannt, T. Francis, M. Mermer, G. Veeraraghavan, Magneto Resistive Elements and Methods for Manufacture and Use of Same, 2011. URL, http://www.google.com/patents/US8077152.

[4] W. Baker, K. Ambal, D. Waters, R. Baarda, H. Morishita, K. van Schooten, D. McCamey, J. Lupton, C. Boehme, Robust absolute magnetometry with organic thin-film devices, Nat. Commun. 3 (2012) 898, http://dx.doi.org/10.1038/ncomms1895.

[5] M. Gobbi, E. Orgiu, The rise of organic magnetoresistance: materials and challenges, J. Mater. Chem. C Adv. http://dx.doi.org/10.1039/C6TC04403D.

[6] J. Zhu, M. Chen, H. Qu, Z. Luo, S. Wu, H.A. Colorado, S. Wei, Z. Guo, Magnetic

field induced capacitance enhancement in graphene and magnetic graphene nanocomposites, Energy Environ. Sci. 6 (1) (2013) 194–204, http://dx.doi.org/10.1039/C2EE23422J.
[7] R. Sadu, N. Haldolaarachchige, D. Chen, D.P. Young, Separating positive and negative magnetoresistance for polyaniline-silicon nanocomposites in variable range hopping regime, Appl. Phys. Lett. 102 (21) (2013) 212403, http://dx.doi.org/10.1063/1.4807787.
[8] H. Gu, J. Guo, X. Yan, H. Wei, X. Zhang, J. Liu, Y. Huang, S. Wei, Z. Guo, Electrical transport and magnetoresistance in advanced polyaniline nanostructures and nanocomposites, Polymer 55 (17) (2014) 4405–4419, http://dx.doi.org/10.1016/j.polymer.2014.05.024.
[9] J. Guo, L. Guan, H. Wei, M.A. Khan, X. Zhang, B. Li, Q. Wang, B.L. Weeks, D.P. Young, T. Shen, S. Wei, Z. Guo, Enhanced negative magnetoresistance with high sensitivity of polyaniline interfaced with nanotitania, J. Electrochem. Soc. 163 (8) (2016) H664–H671, http://dx.doi.org/10.1149/2.0371608jes.
[10] P.A. Bobbert, Organic semiconductors: what makes the spin relax? Nat. Mater. 9 (4) (2010) 288–290, http://dx.doi.org/10.1038/nmat2718.
[11] Z.G. Yu, Spin-orbit coupling, spin relaxation, and spin diffusion in organic solids, Phys. Rev. Lett. 106 (10) (2011) 106602, http://dx.doi.org/10.1103/PhysRevLett.106.106602.
[12] Y. Wu, B. Hu, Metal electrode effects on spin-orbital coupling and magnetoresistance in organic semiconductor devices, Appl. Phys. Lett. 89 (20) (2006) 203510, http://dx.doi.org/10.1063/1.2387118.
[13] J.-Q. Zhao, M. Ding, T.-Y. Zhang, N.-Y. Zhang, Y.-T. Pang, Y.-J. Ji, Y. Chen, F.-X. Wang, G. Fu, The effect of spin-orbit coupling on magnetoresistance in nonmagnetic organic semiconductors, Chin. Phys. B 21 (5) (2012) 057110, http://dx.doi.org/10.1088/1674-1056/21/5/057110.
[14] Y. Sheng, T.D. Nguyen, G. Veeraraghavan, O. Mermer, M. Wohlgenannt, S. Qiu, U. Scherf, Hyperfine interaction and magnetoresistance in organic semiconductors, Phys. Rev. B 74 (4) (2006) 045213, http://dx.doi.org/10.1103/PhysRevB.74.045213.
[15] N.J. Rolfe, M. Heeney, P.B. Wyatt, A.J. Drew, T. Kreouzis, W.P. Gillin, Elucidating the role of hyperfine interactions on organic magnetoresistance using deuterated aluminium tris(8-hydroxyquinoline), Phys. Rev. B 80 (24) (2009) 241201(R), http://dx.doi.org/10.1103/PhysRevB.80.241201.
[16] P.A. Bobbert, T.D. Nguyen, F.W.A. van Oost, B. Koopmans, M. Wohlgenannt, Bipolaron mechanism for organic magnetoresistance, Phys. Rev. Lett. 99 (21) (2007) 216801, http://dx.doi.org/10.1103/PhysRevLett.99.216801.
[17] V.N. Prigodin, J.D. Bergeson, D.M. Lincoln, A.J. Epstein, Anomalous room temperature magnetoresistance in organic semiconductors, Synth. Met. 156 (9–10) (2006) 757–761, http://dx.doi.org/10.1016/j.synthmet.2006.04.010.
[18] J.D. Bergeson, V.N. Prigodin, D.M. Lincoln, A.J. Epstein, Inversion of magnetoresistance in organic semiconductors, Phys. Rev. Lett. 100 (6) (2008) 067201, http://dx.doi.org/10.1103/PhysRevLett.100.067201.
[19] H. Odaka, Y. Okimoto, T. Yamada, H. Okamoto, M. Kawasaki, Y. Tokura, Control of magnetic-field effect on electroluminescence in Alq_3-based organic light emitting diodes, Appl. Phys. Lett. 88 (12) (2006) 123501, http://dx.doi.org/10.1063/1.2185256.
[20] Y. Iwasaki, T. Osasa, M. Asahi, M. Matsumura, Y. Sakaguchi, T. Suzuki, Fractions of singlet and triplet excitons generated in organic light-emitting devices based on a polyphenylenevinylene derivative, Phys. Rev. B 74 (19) (2006) 195209, http://dx.doi.org/10.1103/PhysRevB.74.195209.
[21] P. Desai, P. Shakya, T. Kreouzis, W.P. Gillin, N.A. Morley, M.R.J. Gibbs, Magnetoresistance and efficiency measurements of Alq_3-based OLEDs, Phys. Rev. B 75 (9) (2007) 094423, http://dx.doi.org/10.1103/PhysRevB.75.094423.
[22] V. Ern, R.E. Merrifield, Magnetic field effect on triplet exciton quenching in organic crystals, Phys. Rev. Lett. 21 (9) (1968) 609–611, http://dx.doi.org/10.1103/PhysRevLett.21.609.
[23] B. Hu, Y. Wu, Tuning magnetoresistance between positive and negative values in organic semiconductors, Nat. Mater. 6 (12) (2007) 985–991, http://dx.doi.org/10.1038/nmat2034.
[24] B. Hu, L. Yan, M. Shao, Magnetic-field effects in organic semiconducting materials and devices, Adv. Mater. 21 (14–15) (2009) 1500–1516, http://dx.doi.org/10.1002/adma.200802386.
[25] F.L. Bloom, M. Kemerink, W. Wagemans, B. Koopmans, Sign inversion of magnetoresistance in space-charge limited organic devices, Phys. Rev. Lett. 103 (6) (2009) 066601, http://dx.doi.org/10.1103/PhysRevLett.103.066601.
[26] M. Fayolle, M. Yamaguchi, S.T. Pham, T. Ohto, H. Tada, Determination of the mechanism behind the organic magnetoresistance (OMAR) effect by using impedance spectroscopy, Int. J. Nanotechnol. 12 (3/4) (2015) 238, http://dx.doi.org/10.1504/IJNT.2015.067209.
[27] M. Fayolle, M. Yamaguchi, T. Ohto, H. Tada, Impedance spectroscopy of organic magnetoresistance devices - effect of interface disorder, J. Appl. Phys. 117 (7) (2015) 075501, http://dx.doi.org/10.1063/1.4913272.
[28] W. Wagemans, P. Janssen, E.H.M. van der Heijden, M. Kemerink, B. Koopmans, Frequency dependence of organic magnetoresistance, Appl. Phys. Lett. 97 (12) (2010) 123301, http://dx.doi.org/10.1063/1.3491217.
[29] F. Wang, J. Rybicki, R. Lin, K.A. Hutchinson, J. Hou, M. Wohlgenannt, Frequency dependence of organic magnetoresistance, Synth. Met. 161 (7–8) (2011) 622–627, http://dx.doi.org/10.1016/j.synthmet.2010.11.046.
[30] P. Janssen, W. Wagemans, W. Verhoeven, E. van der Heijden, M. Kemerink, B. Koopmans, On the role of minority carriers in the frequency dependence of organic magnetoresistance, Synth. Met. 161 (7–8) (2011) 617–621, http://dx.doi.org/10.1016/j.synthmet.2011.01.013.
[31] T.K. Djidjou, T. Basel, A. Rogachev, Admittance spectroscopy study of polymer diodes in small magnetic fields, J. Appl. Phys. 112 (2) (2012) 024511, http://dx.doi.org/10.1063/1.4737773.
[32] T.K. Djidjou, T. Basel, A. Rogachev, Magnetic-field dependent differential capacitance of polymer diodes, Appl. Phys. Lett. 101 (9) (2012) 093303, http://dx.doi.org/10.1063/1.4748797.
[33] O. Mermer, G. Veeraraghavan, T.L. Francis, Y. Sheng, D.T. Nguyen, M. Wohlgenannt, A. Köhler, M.K. Al-Suti, M.S. Khan, Large magnetoresistance in nonmagnetic π-conjugated semiconductor thin film devices, Phys. Rev. B 72 (20) (2005) 205202, http://dx.doi.org/10.1103/PhysRevB.72.205202.
[34] A. Einstein, Über die von der molekularkinetischen theorie der wärme geforderte bewegung von in ruhenden flüssigkeiten suspendierten teilchen, Ann. Phys. (Berlin, Ger.) 322 (8) (1905) 549–560, http://dx.doi.org/10.1002/andp.19053220806.
[35] G.A.H. Wetzelaer, L.J.A. Koster, P.W.M. Blom, Validity of the Einstein relation in disordered organic semiconductors, Phys. Rev. Lett. 107 (6) (2011) 066605, http://dx.doi.org/10.1103/PhysRevLett.107.066605.
[36] L. Pautmeier, R. Richert, H. Bässler, Poole-Frenkel behavior of charge transport in organic solids with off-diagonal disorder studied by Monte Carlo simulation, Synth. Met. 37 (1–3) (1990) 271–281, http://dx.doi.org/10.1016/0379-6779(90)90158-H.
[37] J.J.M. van der Holst, F.W.A. van Oost, R. Coehoorn, P.A. Bobbert, Electron-hole recombination in disordered organic semiconductors: validity of the Langevin formula, Phys. Rev. B 80 (23) (2009) 235202, http://dx.doi.org/10.1103/PhysRevB.80.235202.
[38] D.L. Scharfetter, H.K. Gummel, Large-signal analysis of a silicon Read diode oscillator, IEEE Trans. Electron Devices 16 (1) (1969) 64–77, http://dx.doi.org/10.1109/T-ED.1969.16566.
[39] G. Paasch, S. Scheinert, Charge carrier density of organics with gaussian density of states: analytical approximation for the gauss-fermi integral, J. Appl. Phys. 107 (10) (2010) 104501, http://dx.doi.org/10.1063/1.3374475.
[40] S. Laux, Techniques for small-signal analysis of semiconductor devices, IEEE Trans. Electron Devices 32 (10) (1985) 2028–2037, http://dx.doi.org/10.1109/T-ED.1985.22235.
[41] H. Gommans, M. Kemerink, R. Janssen, Negative capacitances in low-mobility solids, Phys. Rev. B 72 (23) (2005) 235204, http://dx.doi.org/10.1103/PhysRevB.72.235204.
[42] J.A. Gómez, F. Nüesch, L. Zuppiroli, C.F.O. Graeff, Magnetic field effects on the conductivity of organic bipolar and unipolar devices at room temperature, Synth. Met. 160 (3–4) (2010) 317–319, http://dx.doi.org/10.1016/j.synthmet.2009.11.020.
[43] F.W. King, Hilbert transforms, no. 124-125 in Encyclopedia of Mathematics and its Applications, Cambridge University Press, Cambridge Eng., New York, 2009.
[44] D.C. Tripathi, A.K. Tripathi, Y.N. Mohapatra, Mobility determination using frequency dependence of imaginary part of impedance (Im Z) for organic and polymeric thin films, Appl. Phys. Lett. 98 (3) (2011) 033304, http://dx.doi.org/10.1063/1.3544935.
[45] S.A. Bagnich, U. Niedermeier, C. Melzer, W. Sarfert, H. von Seggern, Electron-hole pair mechanism for the magnetic field effect in organic light emitting diodes based on poly(paraphenylene vinylene), J. Appl. Phys. 106 (11) (2009) 113702, http://dx.doi.org/10.1063/1.3260249.
[46] E. Tutiš, D. Berner, L. Zuppiroli, Internal electric field and charge distribution in multilayer organic light-emitting diodes, J. Appl. Phys. 93 (8) (2003) 4594–4602, http://dx.doi.org/10.1063/1.1558208.
[47] R. Rohloff, N.B. Kotadiya, N.I. Crăciun, P.W.M. Blom, G.A.H. Wetzelaer, Electron and hole transport in the organic small molecule α-NPD, Appl. Phys. Lett. 110 (7) (2017) 073301, http://dx.doi.org/10.1063/1.4976205.
[48] F. Li, L. Xin, S. Liu, B. Hu, Direct measurement of the magnetic field effects on carrier mobilities and recombination in tris-(8-hydroxyquinoline)-aluminum based light-emitting diodes, Appl. Phys. Lett. 97 (7) (2010) 073301, http://dx.doi.org/10.1063/1.3478014.
[49] T.D. Nguyen, Y. Sheng, J. Rybicki, M. Wohlgenannt, Magnetic field-effects in bipolar, almost hole-only and almost electron-only tris-(8-hydroxyquinoline) aluminum devices, Phys. Rev. B 77 (2008) 235209, http://dx.doi.org/10.1103/PhysRevB.77.235209.
[50] Q. Peng, J. Sun, X. Li, M. Li, F. Li, Investigation of the magnetic field effects on electron mobility in tri-(8-hydroxyquinoline)-aluminum based light-emitting devices, Appl. Phys. Lett. 99 (3) (2011) 033509, http://dx.doi.org/10.1063/1.3615305.
[51] L. Chen, Y. Lei, Q. Zhang, Z. Xiong, Negative magnetoconductance effects in amorphous copper phthalocyanine thin film: trap-assisted bipolaron formation, J. Mater. Chem. C 3 (46) (2015) 12056–12060, http://dx.doi.org/10.1039/C5TC01908G.
[52] Z. Sun, Y. Li, K. Gao, D. Liu, Z. An, S. Xie, Dynamical study of polaron-bipolaron scattering in conjugated polymers, Org. Electron. 11 (2) (2010) 279–284, http://dx.doi.org/10.1016/j.orgel.2009.11.006.
[53] L. Ge, S. Li, T.F. George, X. Sun, Organic electroluminescence channel avoiding triplet excitons, Phys. Lett. A 372 (19) (2008) 3375–3379, http://dx.doi.org/10.1016/j.physleta.2008.01.084.
[54] B. Di, Y. Meng, Y.D. Wang, X.J. Liu, Z. An, Electroluminescence enhancement in polymer light-emitting diodes through inelastic scattering of oppositely charged bipolarons, J. Phys. Chem. B 115 (30) (2011) 9339–9344, http://dx.doi.org/10.1021/jp2006342.
[55] P.A. Lane, X. Wei, Z.V. Vardeny, J. Poplawski, E. Ehrenfreund, M. Ibrahim, A.J. Frank, Absorption studies of charged excitations in α-sexithiophene, in:

SPE/ANTEC 1996, Annual Technical Conference Papers, Taylor & Francis, 1996, pp. 1338–1342.
[56] M. Shao, L. Yan, M. Li, I. Ilia, B. Hu, Triplet-charge annihilation versus triplet-triplet annihilation in organic semiconductors, J. Mater. Chem. C 1 (7) (2013) 1330–1336, http://dx.doi.org/10.1039/C2TC00329E.
[57] M. Cox, P. Janssen, F. Zhu, B. Koopmans, Traps and trions as origin of magnetoresistance in organic semiconductors, Phys. Rev. B 88 (3) (2013) 035202, http://dx.doi.org/10.1103/PhysRevB.88.035202.
[58] S. Barth, P. Müller, H. Riel, P.F. Seidler, W. Rieß, H. Vestweber, H. Bässler, Electron mobility in tris(8-hydroxy-quinoline)aluminum thin films determined via transient electroluminescence from single- and multilayer organic light-emitting diodes, J. Appl. Phys. 89 (7) (2001) 3711–3719, http://dx.doi.org/10.1063/1.1330766.
[59] J.Y. Song, N. Stingelin, A.J. Drew, T. Kreouzis, W.P. Gillin, Effect of excited states and applied magnetic fields on the measured hole mobility in an organic semiconductor, Phys. Rev. B 82 (8) (2010) 085205, http://dx.doi.org/10.1103/PhysRevB.82.085205.